Biosensors and Bioelectronics 109 (2018) 13–19

Contents lists available at ScienceDirect

Biosensors and Bioelectronics

journal homepage: www.elsevier.com/locate/bios

Ultrasensitive Faraday cage-type electrochemiluminescence assay for femtomolar miRNA-141 via graphene oxide and hybridization chain reaction-assisted cascade amplification

Jing Lu, Lin Wu, Yufang Hu, Sui Wang, Zhiyong Guo*

School of Materials Science and Chemical Engineering, Ningbo University, Ningbo 315211, PR China

ARTICLE INFO

Keywords:
Electrochemiluminescence biosensor
MiRNA-141
Faraday cage-type ECL biosensor
Hybridization chain reaction

ABSTRACT

In this study, a novel electrochemiluminescence (ECL) biosensor for sensitive detection of femtomolar miRNA-141 was constructed on the basis of Faraday cage-type strategy via graphene oxide (GO) and hybridization chain reaction (HCR)-assisted cascade amplification. A capture probe (CP) was immobilized on Fe_3O_4@SiO_2@Au nanoparticles as capture unit, which could catch the miRNA-141, and the immobilization of the signal unit (Ru(phen)$_3^{2+}$-HCR/GO) was allowed via nucleic acid hybridization. The prepared biosensor exhibited two advantages for signal amplification: firstly, GO could lap on the electrode surface directly, extending Outer Helmholtz Plane (OHP) of the sensor due to the large surface area and good electronic transport property; secondly, HCR-assisted cascade amplification was designed by anchoring all HCR products on the GO surface, then embedding Ru(phen)$_3^{2+}$ as a signal readout pathway. All these signal molecules could take part in electrochemical reactions, thus further enhancing the ECL signal drastically. Therefore, the proposed sensor constructed by integrating HCR with Faraday cage-type strategy displayed an ultrasensitive detection platform for the miRNA-141 with a low detection limit of 0.03 fM. In addition, this proposed biosensor provides a universal platform for analysis of other microRNAs.

1. Introduction

MicroRNAs (miRNAs) are a class of single-strand, short, and endogenous noncoding RNAs with approximately 19–23 nucleotides (Dong et al., 2013; Graybill and Bailey, 2016). It has been demonstrated that the expression levels of miRNAs are directly related to diverse cancers (Garzon et al., 2009; Jou et al., 2015; Lu et al., 2005). Thus, miRNAs possess the potential to be employed as valuable biomarkers for molecular diagnosis of tumors. However, as the concentration of the miRNAs during the process of disease diagnosis is usually very low, higher sensitive methods for the detection of these biomolecules are still in demand (Cissell et al., 2007). Thus, new methods were developed to improve the sensitivity such as fluorescence (Yang et al., 2012; Yin et al., 2012), electrochemiluminescence (Wang et al., 2018; Lu et al., 2018; J.L. Liu et al., 2017; Q. Liu et al., 2017; Nie et al., 2017), surface plasmon resonance (Li et al., 2017; Wang et al., 2016) and electrochemistry (Labib et al., 2016; Wu et al., 2015) ones. Among them, electrochemiluminescence (ECL) biosensors have received many attentions due to their simplicity, low cost and high sensitivity for the detection of miRNAs (Chen et al., 2015; Wu and Qu, 2015).

At present, sandwich-type ECL biosensor is the commonly used mode of ECL biosensor (Cheng et al., 2014; Guo et al., 2017). Nevertheless, low electrode reaction efficiency and small labelling amount of electrochemiluminophores are two main keys that limit the enhancement of sensitivity of the traditional sandwich-type ECL biosensor for the detection of miRNAs to some extent (Liu et al., 2007; Oh et al., 2009; Rashidnadimi et al., 2008). Recently, hybridization chain reaction (HCR) has shown great potential in nucleic acid detection (Shimron et al., 2012; Wang et al., 2011, 2012). HCR is an enzyme-free amplification technique by which the initiator can trigger hybridization and results in the polymerization of oligonucleotides into long nicked dsDNA polymers at mild conditions, which has the capacity to intercalate some small luminescence molecules into its grooves (Dirks and Pierce, 2004; Venkataraman et al., 2007; Chen et al., 2012). DNA-based HCR methods for amplified ECL signal to detect the DNA/RNA have been reported (Gui et al., 2013). It indicates that HCR has been an ideal choice for miRNAs detection. Nevertheless, a simple HCR signal amplification is still not easy to further improve the detection sensitivity, which displays insufficient signal output on the electrode surface.

With the development of nanotechnology, graphene oxide (GO) has

* Corresponding author.
E-mail address: guozhiyong@nbu.edu.cn (Z. Guo).

https://doi.org/10.1016/j.bios.2018.02.062
Received 6 December 2017; Received in revised form 27 February 2018; Accepted 27 February 2018
Available online 06 March 2018
0956-5663/

been applied in the ECL field to improve analytical performance (Dong et al., 2016; Feng et al., 2016). GO presents many excellent properties such as abundant functional groups, good electronic transport property and large surface area which can easily load plenty of antibodies, enzymes, DNAs and various labels. Benefitting from these excellent properties, we have proposed a new concept of Faraday cage-type model based on GO, which can overcome the low electrode reaction efficiency (Guo et al., 2016). In Faraday cage-type ECL biosensor, the GO in the signal unit extends the Outer Helmholtz Plane (OHP) of the electrode, making all the electrochemiluminophores labeled effective as such that they are immobilized directly on the surface of the electrode or even "in the electrode". In this case of the state, the signal unit overlapped with the electrode surface directly, so electrons could flow freely between the signal unit and the electrode. In other words, the signal unit becomes a part of the electrode. All electrochemiluminophores labeled on the signal unit were on the surface of the "Faraday cage", so all of them could take part in the electrode reaction to emit ECL signals, profiting from the free flow of electrons resulting from the isopotential character of the "Faraday cage". Thus, the sensitivity of ECL was improved greatly to detect fg level of target protein (Guo et al., 2016). Up to now, even though GO and HCR have been applied for the construction of sensing interface, there is not a report that integrates GO and HCR for the application in Faraday-cage ECL assay yet.

In this study, GO was employed to immobilize trigger probe (TP) to obtain the TP/GO. In the presence of hairpin DNA 2 (H2) and hairpin DNA 1 (H1) that is partially complementary to both H2 and TP, it could in situ propagate chain reaction of hybridization events to obtain dsDNA. Numerous electrochemiluminophores $Ru(phen)_3^{2+}$ insert the DNA grooves to form the $Ru(phen)_3^{2+}$-HCR/GO complex as signal unit (Xu and Bard, 1995; Tang et al., 2010; Yin et al., 2009). After the miRNA-141 hybridization, the signal unit could be fixed onto the electrode surface to form a Faraday cage-type structure. In this strategy, the electrons could flow freely from the electrode to the signal unit. All electrochemiluminophores $Ru(phen)_3^{2+}$ immobilized on the signal unit can take part in electrode reactions to emit ECL signals, thus greatly improving electrode reaction efficiency. Coupling with increased electrochemiluminophores amounts through HCR, the two keys that restrict the sensitivity improvement of sandwich-type ECL biosensor were substantially eliminated, and the tactic opens up new opportunities for fast, simple and sensitive analysis of miRNAs.

2. Experimental

2.1. Reagents and materials

All DNA and RNA oligonucleotides were synthesized and HPLC-purified by Sangon Biotechnology Co., Ltd. (Shanghai, China) with their sequences listed in Table S1. Ammonium persulfate (APS), 40% acrylamide mix solution, 1,2-bis(dimethylamino)-ethane (TEMED), and low range DNA ladder were obtained from Sangon too. Ferric chloride hexahydrate ($FeCl_3{\cdot}6H_2O$), ammonium hydroxide (NH_4OH, 25 wt%), sodium citrate, ammonium acetate (NH_4Ac), tetraethoxylsilane (TEOS, > 98%) and hydrogen tetrachloroaurate (III) hydrate ($HAuCl_4{\cdot}4H_2O$) were purchased from Sinopharm Chemical Reagent Co., Ltd. (Shanghai, China). Tetrakis (hydroxymethyl) phosphonium chloride (THPC) was obtained from TCI Development Co., Ltd. (Shanghai, China). Tris (2-carboxyethyl) phosphine hydrochloride (TCEP), 6-mercapto-1-hexanol (MCH), 1-ethyl-3-(3-(dimethylamino) propyl) carbodiimide (EDC), N-hydroxysuccinimide (NHS) and 2-(dibutylamino) ethanol (DBAE) were purchased from Sigma-Aldrich (St. Louis, MO, USA). Dichlorotris(1,10-phenanthroline) ruthenium hydrate ($Ru(phen)_3Cl_2{\cdot}H_2O$) and (3-Aminopropyl) triethoxysilane (APTES) were purchased from Aladdin (Shanghai, China). Buffers involved in this work are shown in Supporting Information 1.

2.2. Apparatus

ECL measurements were performed with a custom-built ECL detection system that mainly contains a BPCL ultra-weak chemiluminescence analyzer (Institute of Biophysics, Chinese Academy of Sciences, Beijing, China) and a CHI 1100 A electrochemical workstation (Chenhua Instrument Company, Shanghai, China). A three-electrode system was used, containing a bare or modified magnetic glassy carbon electrode (MGCE, 3 mm diameter, GaossUnion, Wuhan, China) as working electrode, a platinum wire electrode as counter electrode and an Ag/AgCl (3 M KCl) electrode as reference electrode. Electrochemical impedance spectroscopy (EIS) analysis was carried out by using a CHI 660E electrochemistry workstation (Chenhua Instrument Company, Shanghai, China). Polyacrylamide gelelectrophoresis (PAGE) was scanned by a ChemiDoc™ MP System (Bio-Rad, USA). The morphologies of nanomaterials were characterized by using Hitachi SU-70 scanning electron microscope (SEM, Hitachi, Tokyo, Japan). Fourier transform infrared (FTIR) spectra were recorded on a Nicolet AVATAR FTIR 6700 spectrometer. The X-ray photoelectron spectroscopy (XPS) spectra were measured by AXIS Ultra spectrometer (Shimadzu, Japan).

2.3. Synthesis of capture unit (Fe_3O_4@SiO_2@AuNPs-CP)

Fe_3O_4@SiO_2@Au nanoparticles (Fe_3O_4@SiO_2@AuNPs) were prepared as previously reported (Jiang et al., 2013; Liu et al., 2014). These steps were shown in the Supporting Information 2. The Fe_3O_4@SiO_2@AuNPs were dispersed in probe immobilization buffer with the concentration of 1 mg/mL. Later, 25 μL of 5 μM thiol modified hairpin capture probe (CP) was blended with 100 μL of 1 mg/mL Fe_3O_4@SiO_2@AuNPs. The mixture was left undisturbed in the dark for 16 h, followed by adding 10 μL of 10 mM MCH for 40 min to block non-specific sites. After washing and reconstructing in 100 μL of DNA hybridization buffer, the Fe_3O_4@SiO_2@AuNPs-CP, denoted as capture unit was obtained.

2.4. Preparation of signal unit ($Ru(phen)_3^{2+}$-HCR/GO)

The preparation of GO was custom-synthesized by Hummer's method (Hummers and Offeman, 1958). Details of the preparation can be found in Supporting Information 3. The carboxylic groups on GO surface were activated by using EDC and NHS for 1 h at room temperature. Subsequently, 20 μL of 1 μM TP was added into 200 μL of 1 mg/mL activated GO, incubated for 4 h to obtain TP/GO through amino-carboxyl reaction and reconstructed to 100 μL. After that, 10 μL of 1 μM H1 and 10 μL of 1 μM H2 solution were simultaneously added into 100 μL of TP/GO and reacted for 2 h. In the presence of H1 and H2 which is partially complementary to H1, dsDNA could be obtained through in situ HCR (Supporting Information 4) and then HCR/GO was obtained. Finally, a droplet of 10 μL of 20 mM $Ru(phen)_3^{2+}$ was added in the HCR/GO solution and incubated for 7 h. In this process, numerous $Ru(phen)_3^{2+}$ can be efficiently intercalated into the grooves of the dsDNA to form $Ru(phen)_3^{2+}$-HCR/GO complex (Supporting Information 5). After incubation, the solution was rinsed three times to remove the excessive $Ru(phen)_3^{2+}$ and the signal unit $Ru(phen)_3^{2+}$-HCR/GO was obtained.

2.5. Fabrication of the ECL biosensor

The assembly process of the modified electrode is illustrated in Scheme 1. Prior to sensor fabrication, the MGCE was polished to a mirror with 1.0, 0.3 and 0.05 μm alumina slurry, washed ultrasonically in water, and allowed to dry in N_2. Then 10 μL of as-prepared capture unit was dropped and firmly attached to the surface of the MGCE by magnet. A 5 μL of different concentrations of target miRNA was dropped onto the resulting electrode to hybridize with the hairpin CP in the capture unit at 37 °C for 60 min. Afterwards, the electrode was

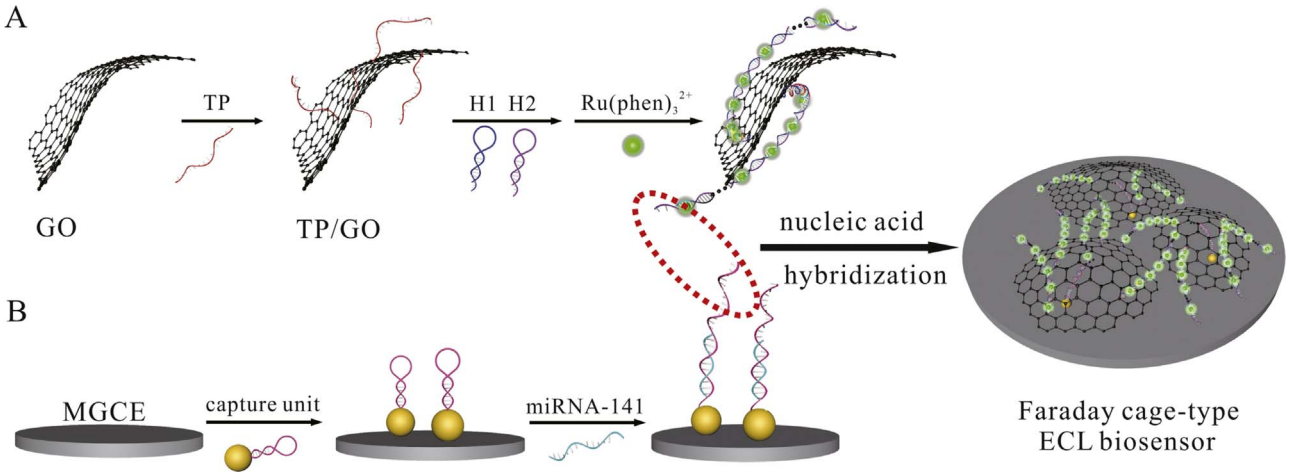

Scheme 1. Schematic diagram of (A) the preparation procedure of the signal unit and (B) the fabrication of the proposed ECL biosensor for miRNA-141 detection.

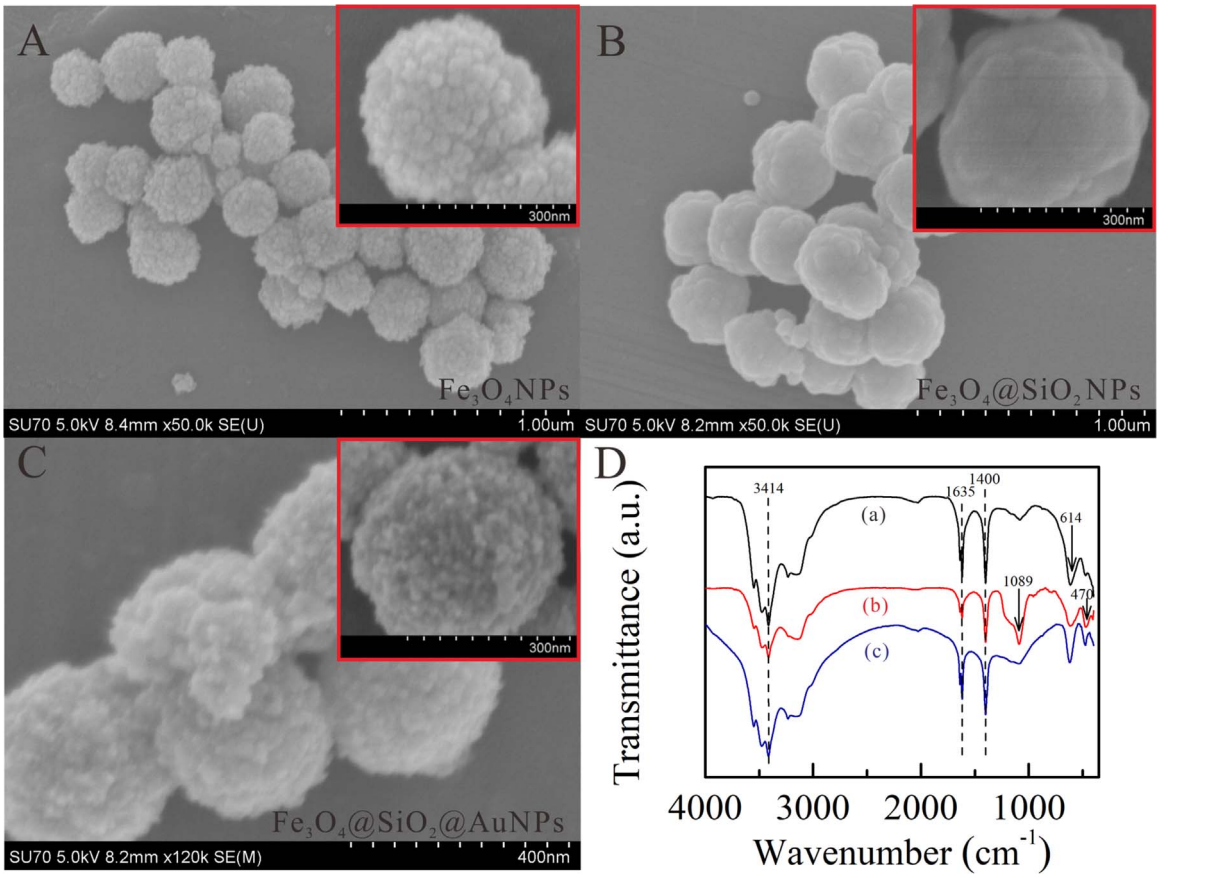

Fig. 1. SEM images of (A) Fe_3O_4NPs, (B) Fe_3O_4@SiO_2NPs, and (C) Fe_3O_4@SiO_2@AuNPs, as well as (D) FTIR spectra of (a) Fe_3O_4NPs, (b) Fe_3O_4@SiO_2NPs, and (c) Fe_3O_4@SiO_2@AuNPs.

rinsed with miRNA hybridization buffer again and incubated with 5 μL of signal unit at 37 °C for 1 h. After being rinsed with miRNA hybridization buffer, the Faraday cage-type ECL biosensor was obtained and the electrochemical signal was detected in ECL working buffer. All the experiments were performed under room temperature.

2.6. ECL detection

The Faraday cage-type ECL biosensor was scanned using chronoamperometry (30 s pulse period, 0.25 s pulse width, 0 V initial potential, 1.2 V pulse potential) in the ECL working buffer, with 0.1 M PBS at pH 7.4 containing 20 mM DBAE as a coreactant. In addition, the ECL signal was recorded with the voltage of a photomultiplier tube (PMT) at 900 V in the process of detection.

3. Results and discussion

3.1. Principle of the Faraday cage-type ECL biosensor

The principle of ECL biosensor for sensitive detection of miRNA-141 is shown in Scheme 1. The biosensor mainly consists of signal unit and capture unit. The formation of signal unit includes three steps (Scheme 1A): firstly, GO was employed to immobilize TP to obtain the TP/GO via chemical bonding of amino-carboxyl interaction. Then, two hairpins

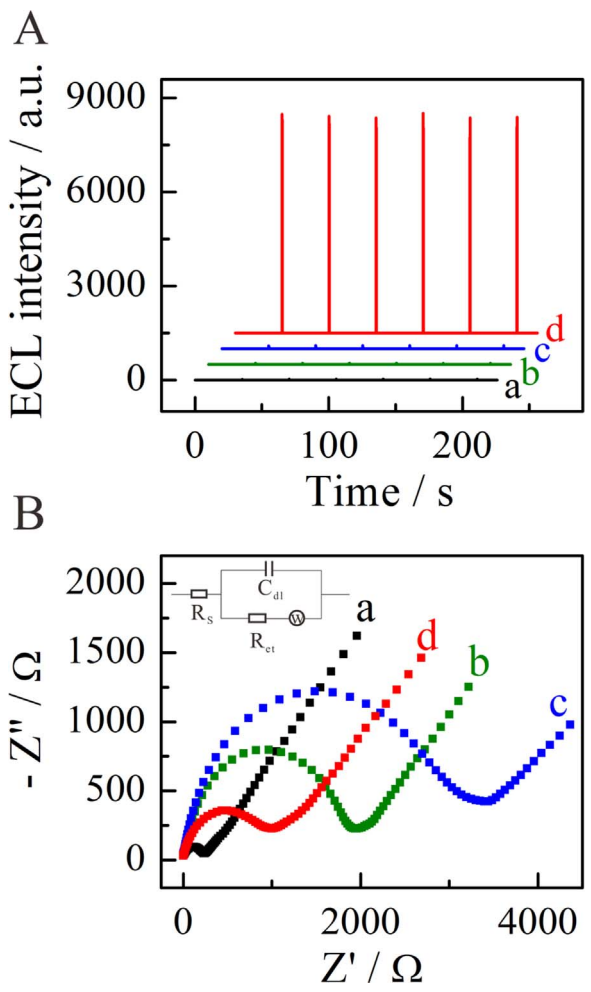

Fig. 2. ECL (A) and EIS (B) profiles of (a) the bare MGCE, (b) (a) + capture unit, (c) (b) + miRNA-141, and (d) (c) + signal unit. Experimental conditions of ECL: chronoamperometry; initial potential, 0 V; pulse potential, 1.2 V; pulse width, 0.25 s; pulse period, 30 s; DBAE, 20 mM; PBS, 0.1 M, and pH 7.4. Experimental conditions of EIS: Fe $(CN)_6^{3-/4-}$, 5 mM; PBS, 0.05 M and pH 7.4.

DNA of H1 and H2 were introduced to TP/GO solution, which could in situ propagate chain reaction of hybridization events to obtain dsDNA in presence of TP. Finally, a lot of $Ru(phen)_3^{2+}$ molecules were intercalated into the dsDNA polymers to obtain $Ru(phen)_3^{2+}$-HCR/GO. Benefitting from the HCR, the DNA skeleton could be extended to absorb more $Ru(phen)_3^{2+}$, leading to a large increasement of electrochemiluminophores. The capture unit was prepared by immobilizing CP on Fe_3O_4@SiO_2@AuNPs, which could easily capture target miRNA-141 and be attracted onto the surface of the MGCE by magnetic force. In the presence of target miRNA-141, it hybridized with CP and opened CP stem-loop structure to form a partial dsDNA, as well as making the end residues sequence of CP to couple with H2 that exposed on the signal unit and finally leading to the successful immobilization of the signal unit. After the signal unit was directly fixed onto the electrode surface to form a Faraday cage-type structure, it is just like a huge net and even becomes a part of the electrode surface. OHP was extended and all Ru $(phen)_3^{2+}$ immobilized on the signal unit can take part in the electrode reaction to emit ECL signals, thus it provided two-stage amplification for the final ECL signal. With the help of HCR and Faraday cage-type strategy, the ECL signal for the detection of miRNA-141 could be amplified remarkably. The higher the concentration of miRNA-141 was, the more signal units were combined, the more $Ru(phen)_3^{2+}$ were bound accordingly, and thus, the higher ECL intensities were obtained. Therefore, the concentration of miRNA can be detected by monitoring the change in ECL signal intensities.

3.2. Characterization of the nanomaterials

The morphologies of the prepared Fe_3O_4 nanoparticles (Fe_3O_4NPs), Fe_3O_4@SiO_2 nanoparticles (Fe_3O_4@SiO_2NPs) and Fe_3O_4@SiO_2@AuNPs, were investigated by SEM, as shown in Fig. 1. From Fig. 1A, it can be clearly seen that Fe_3O_4NPs are uniform spherical particles with the mean diameter about 300 nm, with the surface being not so smooth. After being coated with a silica layer, the surface of Fe_3O_4@SiO_2NPs becomes smooth (Fig. 1B). Au-coated Fe_3O_4@SiO_2NPs were formed with many little Au nanoparticles adhered to the surface of the Fe_3O_4@SiO_2 microsphere, resulting in a little rougher surface (Fig. 1C).

Representative FTIR spectra for Fe_3O_4NPs, Fe_3O_4@SiO_2NPs and Fe_3O_4@SiO_2@AuNPs are shown in Fig. 1D. Curve a shows the FTIR spectrum of Fe_3O_4NPs, in which the characteristic peak appearing at 614 cm^{-1} can be seen. The peak is ascribed to the Fe-O stretching vibration. In addition, there are new strong bands around 470 cm^{-1} to 1089 cm^{-1} originating from the Fe-O-Si and Si-O bond of silica (curve b). This result indicates that SiO_2 is immobilized on the surface of Fe_3O_4NPs. Curve c shows the FTIR spectrum of Fe_3O_4@SiO_2@AuNPs. The characteristic peak of Fe_3O_4@SiO_2@AuNPs is almost the same as that of Fe_3O_4@SiO_2 because Au nanoparticles do not have absorption in the infrared region. To further demonstrate the formation of Fe_3O_4@SiO_2@AuNPs, XPS was employed to examine the surface of the Fe_3O_4@SiO_2@AuNPs. It is clear that the elemental contents of the surface are Au, Si, O, and Fe (Fig. S3). The binding energy at 707.05 eV for Fe 2p3 cannot be detected, suggesting that all the Fe_3O_4NPs cores are confined within a shell of SiO_2@AuNPs. Besides, the binding energy of Si 2p6 is not remarkable in the XPS spectra, and the peak at 80.7 eV resulting from the AuNPs is intensive, indicating that the Fe_3O_4@SiO_2NPs are coated by AuNPs. All results above suggest that Fe_3O_4@SiO_2@AuNPs were successfully prepared.

3.3. Characterization of the Faraday cage-type ECL biosensor

3.3.1. ECL behavior

The ECL signal was recorded step by step to monitor the behavior of the electrode modification. As can be seen in Fig. 2A, no detectable signal was observed on bare MGCE (curve a), capture unit/MGCE (curve b), or miRNA-141/capture unit/MGCE (curve c), respectively. However, after being incubated with a signal unit, a sharp ECL response appeared at the signal unit/miRNA-141/capture unit/MGCE (curve d), corresponding to the intercalation of $Ru(phen)_3^{2+}$ into the dsDNA skeletons and the formation of Faraday cage-type ECL biosensor.

3.3.2. EIS behavior

EIS measurement of $[Fe(CN)_6]^{3-/4-}$ solution is a valuable and convenient method to give more detailed information of the electrode surface during the fabrication process. In EIS, the semicircle diameter in the impedance spectrum is equal to the electron-transfer resistance, R_{et}. As shown in Fig. 2B, a very small semicircle domain was achieved when bare MGCE was detected (curve a), indicating excellent electron transfer capability. After the capture unit was immobilized onto the MGCE, the diameter of the semicircle increased (curve b); the value of resistance is about 2000 Ω. When miRNA-141 hybridized with capture probe, R_{et} (curve c) increased further because the miRNA-141 formed an additional barrier and further prevented the redox probe from the electrode surface. However, when the signal unit was immobilized on the electrode surface, GO in the signal unit overlapped with the electrode surface directly as if becoming a part of the electrode and thus building the Faraday cage-type ECL biosensor. Therefore, electrons could transfer freely from the electrode to the signal unit without the hindrance of the capture unit and miRNA-141, thus, R_{et} significantly decreased to about 1000 Ω (curve d).

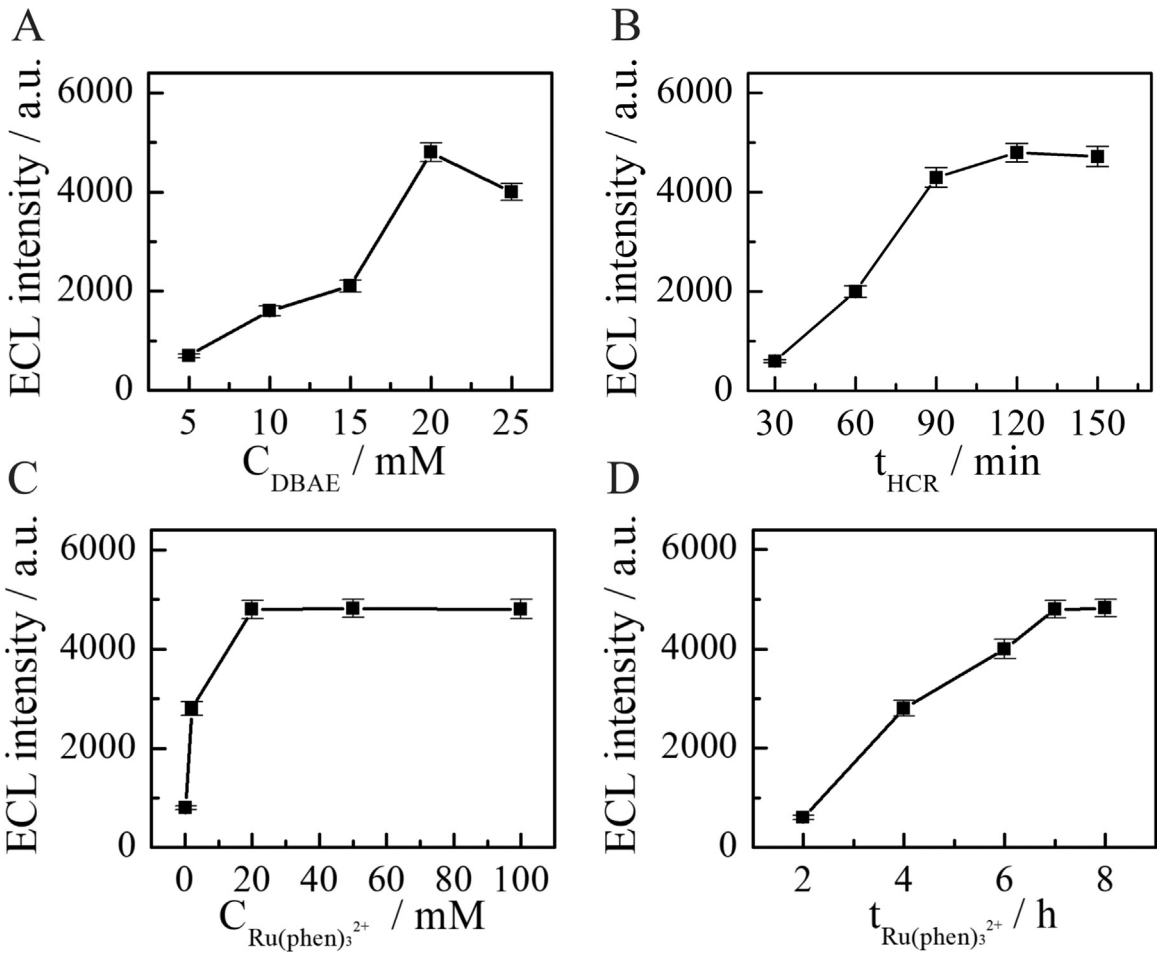

Fig. 3. Effect of (A) DBAE concentration in the ECL detection solution, (B) HCR hybridization time, (C) $Ru(phen)_3^{2+}$ concentration used, and (D) the inset time of $Ru(phen)_3^{2+}$ via HCR on the ECL intensity.

3.4. Optimization of experimental conditions

Experimental conditions were optimized to maximize the sensitivity and efficiency of the biosensor using 5 fM miRNA-141. DBAE served as a coreactant in the ECL of $Ru(phen)_3^{2+}$, the concentration of which would influence the performance of the ECL biosensor greatly. Fig. 3A shows the effect of DBAE concentration on the electrode response. The ECL signal increased gradually with DBAE concentration and reached the maximum at 20 mM. Hence, 20 mM was chosen as the appropriate DBAE concentration. Further, the incubation time of H1 and H2 would affect the HCR triggering, which may influence the ECL signal intensity. Thus, the incubation time of H1 and H2 (t_{HCR}) was investigated, and the results obtained (Fig. 3B) showed that, with the increase of incubation time, ECL intensity increased and then reached the maximum value at 120 min. Therefore, 120 min was selected as the best incubation time of H1 and H2.

In this work, the ECL signal mainly derives from the HCR reaction to introduce $Ru(phen)_3^{2+}$ as signal molecules. Thus, the $Ru(phen)_3^{2+}$ concentration used and the immobilization time of $Ru(phen)_3^{2+}$ via HCR are expected to affect the response signal. Fig. 3C depicts a correlation relationship between $Ru(phen)_3^{2+}$ concentration and ECL intensity. When it was more than 20 mM, the ECL intensities were barely changed. So, 20 mM is employed as the optimal $Ru(phen)_3^{2+}$ concentration. Because $Ru(phen)_3^{2+}$ molecules were intercalated into the dsDNA polymers, the inset time of $Ru(phen)_3^{2+}$ via HCR should be optimized too. As shown in Fig. 3D, with the inset time of $Ru(phen)_3^{2+}$ increasing, the ECL intensity increased with it and then reached a stable state after 7 h. Therefore, the inset time of $Ru(phen)_3^{2+}$ of 7 h was selected.

3.5. Analytical performance of the biosensor for miRNA-141 detection

Under the optimal conditions, ECL intensities were recorded after the proposed biosensors were incubated in different concentrations of miRNA-141. It can be found from Fig. 4A that the ECL intensity increased with the increase of miRNA-141 concentration and showed a good linear relationship versus the logarithm of miRNA-141 concentrations in the range from 0.1 fM to 1 pM (Fig. 4B). The line regression equation is $y = 3027.3 + 2406.5 \times \log x$ with a correlation coefficient of 0.990 in which y is the ECL intensity and x is the miRNA-141 concentration. The limit of detection (LOD) is estimated as 0.03 fM (LOD = $3S_B/m$, where m is the slope of the corresponding calibration curve and S_B is the standard deviation of the blank). As shown in Table 1, this proposed biosensor showed much better performance in sensitivity compared with the previously reported biosensors for the detection of miRNAs (Azimzadeh et al. 2016; Chang et al. 2017; Xu et al. 2017; Zhang et al. 2016; H. Zhang et al. 2015; P. Zhang et al. 2015; Zhou et al. 2017), attributing to the special Faraday cage-type strategy via GO and hybridization chain reaction (HCR)-assisted cascade amplification.

3.6. Stability and selectivity of the biosensor for miRNA-141 detection

To evaluate the stability of the proposed biosensor, the ECL emission from the Faraday cage-type ECL biosensor incubated in 50 fM miRNA-141 was recorded under continuous potential scanning for 15

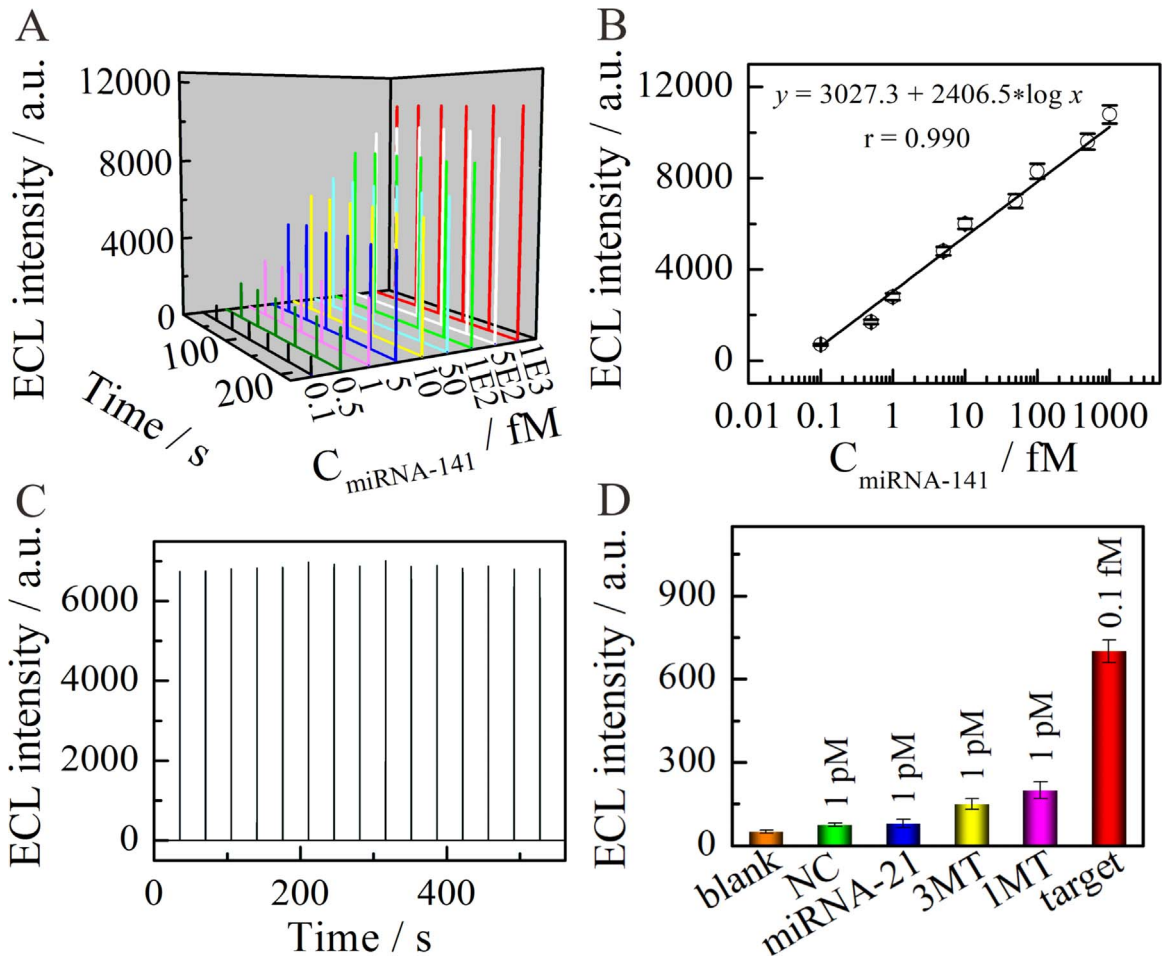

Fig. 4. (A) ECL intensity of the Faraday cage-type ECL biosensor incubated with different concentrations of miRNA-141: 0.1, 0.5, 1, 5, 10, 50, 100, 500, and 1000 fM; (B) The calibration curve obtained through plotting ECL intensity against the logarithmic concentrations of miRNA-141 (fM); (C) ECL stability of the Faraday cage-type ECL biosensor incubated in 50 fM miRNA-141 under continuous chronoamperometry for 15 cycles; (D) Selectivity of the Faraday cage-type ECL biosensor incubated in blank, 1.0 pM noncomplementary sequences (NC), 1.0 pM miRNA-21, 1.0 pM three-base mismatch target (3MT), 1.0 pM signal-base mismatch target (1MT) and 0.1 fM target miRNA-141.

Table 1
Comparison of main methods reported for the determination of miRNAs.

Analytical methods	Target miRNAs	Detection limit	Linear range	References
DPV	miRNA-155	0.6 fM	2.0 fM–8.0 pM	Azimzadeh et al. (2016)
DPV	miRNA-21	1.92 fM	0.5 fM–5.0 pM	Zhang et al. (2016)
SWV	miRNA-182-5p	0.5 fM	1.0 fM–500.0 pM	Chang et al. (2017)
FL	miRNA-155	100 pM	0.1 nM–200 nM	H. Zhang et al. (2015)
SERS	miRNA-21	10 fM	0.1 pM–100 nM	Zhou et al. (2017)
ECL	miRNA-141	3.3 fM	10 fM–100 pM	Xu et al. (2017)
ECL	miRNA-151	0.83 fM	2.5 fM–50 pM	P. Zhang et al. (2015)
ECL	miRNA-141	0.03 fM	0.1 fM–1 pM	This work

DPV: Differential Pulse Voltammetry; SWV: Square-Wave Voltammetry; FL: Fluorescence; SERS: Surface-Enhanced Raman Spectroscopy; ECL: Electrochemiluminescence.

cycles as shown in Fig. 4C. The ECL signals were high and stable, suggesting that the biosensor was suitable for ECL detection. Moreover, the capture unit and signal unit solution were stored at 4 °C in a refrigerator. After two weeks of storage period, the ECL intensity for the detection of 50 fM miRNA-141 was 92.4% of the initial value, which was obtained when the sensor were constructed freshly. Thus, the biosensor has acceptable storage stability.

To assess the specificity of the biosensor, four different kinds of control miRNA sequences including miRNA-21, non-complementary sequence (NC), three-base mismatched target (3MT), and single-base mismatched target (1MT) were evaluated under the same experimental conditions. Compared with the blank test, there was almost no difference in ECL response in the detection of miRNA-21, NC, 3MT and 1 MT at the concentration of 1.0 pM shown in Fig. 4D. However, when the biosensor was incubated with 0.1 fM miRNA-141, a much higher ECL response was achieved. The result indicated the high specificity of this biosensor for miRNA-141.

3.7. Reproducibility and precision of the biosensor for miRNA-141 detection

To assess the reproducibility of the as-developed sensor, five electrodes were fabricated independently by the same procedure as described in Section 2.5. The relative standard deviation (RSD) is 7.9% for 1 fM miRNA-141 that demonstrates the appropriate reliability of the fabrication procedure.

The precision of the sensor was investigated by detecting two

concentrations of miRNA-141 (1 fM and 100 fM) in five independent series on the same day (intra-day precision) and five consecutive days (inter-day precision). RSD values were 7.3% (1 fM) and 8.2% (100 fM) for intra-day and 9.2% (1 fM) and 8.7% (100 fM) for inter-day precision. The low RSD values of intra-day and inter-day indicate a high precision of the developed sensor.

3.8. Application of the biosensor for real samples

The application and reliability of the proposed ECL biosensor was investigated by determining spiked miRNA-141 samples with different concentrations. The samples were prepared by adding synthetic miRNA-141 solution to blank human serum. As shown in Table S2, the results show an acceptable recovery in the range of 92.1–110.0% and RSD in the range of 6.4–11.8%, indicating that the proposed ECL biosensor is promising and has potential applications in the analysis of clinical samples.

4. Conclusions

In conclusion, a novel ECL biosensor for miRNA detection was developed in this work by combining the advantages of HCR with Faraday cage-type biosensor strategy. In the ECL biosensor, (1) the DNA skeleton could be extended to absorb more $Ru(phen)_3^{2+}$ by HCR in the signal unit, leading to significantly amplified ECL signal; (2) due to the large surface area of GO, the multiple HCR products can be anchored on the GO surface, achieving cascade signal amplification; (3) GO-based outer layer can extend Outer Helmholtz Plane of the electrode, and all the $Ru(phen)_3^{2+}$ molecules of the signal unit could take part in electrode reaction via Faraday cage-type strategy. The proposed biosensor provides a new signal amplification strategy in ECL biosensor with the detection limit as low as 0.03 fM. In addition, the specificity, stability, reproducibility, precision and application of this biosensor were validated. Therefore, this biosensor has an application potential in clinical diagnostics and research.

Acknowledgements

Financial support from the Science and Technology Department of Zhejiang Province of China (2016C33176), the Natural Science Foundation of China (41576098, 81773483, 21605089), the Ningbo Municipal Natural Science Foundation (2017A610228), the Open Subject of State Key Laboratory of Chemo/Biosensing and Chemometrics (2016001) and Project of Academic Research Foundation of Ningbo University (XYL17002) are gratefully acknowledged. This work was also sponsored by K.C. Wong Magna Fund in Ningbo University.

Appendix A. Supporting information

Supplementary data associated with this article can be found in the online version at http://dx.doi.org/10.1016/j.bios.2018.02.062.

References

Azimzadeh, M., Rahaie, M., Nasirizadeh, N., Ashtari, K., Naderi-Manesh, H., 2016. Biosens. Bioelectron. 77, 99–106.
Chang, Y.Y., Zhou, Y., Chai, Y.Q., Yuan, R., 2017. Anal. Chem. 89, 8266–8272.
Chen, Y., Xiang, Y., Yuan, R., Chai, Y.Q., 2015. Anal. Chim. Acta 891, 130–135.
Chen, Y., Xu, J., Su, J., Xiang, Y., Yuan, R., Chai, Y.Q., 2012. Anal. Chem. 84, 7750–7755.
Cheng, Y., Lei, J.P., Chen, Y.L., Ju, H.X., 2014. Biosen. Bioelectron. 51, 431–436.
Cissell, K.A., Shrestha, S., Deo, S.K., 2007. Anal. Chem. 79, 4755–4761.
Dirks, R.M., Pierce, N.A., 2004. Proc. Natl. Acad. Sci. USA 101, 15275–15278.
Dong, H.F., Lei, J.P., Ding, L., Wen, Y.Q., Ju, H.X., Zhang, X.J., 2013. Chem. Rev. 113, 6207–6233.
Dong, Y.P., Chen, G., Zhou, Y., Zhu, J.J., 2016. Anal. Chem. 88, 1922–1929.
Feng, Q.M., Shen, Y.Z., Li, M.X., Zhang, Z.L., Zhao, W., Xu, J.J., Chen, H.Y., 2016. Anal. Chem. 88, 937–944.
Garzon, R., Calin, G.A., Croce, C.M., 2009. Annu. Rev. Med. 60, 167–179.
Graybill, R.M., Bailey, R.C., 2016. Anal. Chem. 88, 431–450.
Guo, Z.Y., Sha, Y.H., Hu, Y.F., Wang, S., 2016. Chem. Commun. 52, 4621–4624.
Guo, Z., Wu, L., Hu, Y.F., Wang, S., Li, X., 2017. Biosens. Bioelectron. 95, 27–33.
Gui, G.F., Zhuo, Y., Chai, Y.Q., Liao, N., Zhao, M., Han, J., Zhu, Q., Yuan, R., Xiang, Y., 2013. Biosens. Bioelectron. 47, 524–529.
Hummers, W.S., Offeman, R.E., 1958. J. Am. Chem. Soc. 80, 1339.
Jiang, H.R., Zeng, X., Xi, Z.J., Liu, M., Li, C.Y., Li, Z.Y., Jin, L., Wang, Z.F., Deng, Y., He, N.Y., 2013. J. Biomed. Nanotechnol. 9, 674–684.
Jou, A.F., Lu, C.H., Ou, Y.C., Wang, S.S., Hsu, S.L., Willner, I., Ho, J.A., 2015. Chem. Sci. 6, 659–665.
Labib, M., Sargent, E.H., Kelley, S.O., 2016. Chem. Rev. 116, 9001–9090.
Li, Q., Wang, Q., Yang, X.H., Wang, K.M., Zhang, H., Nie, W.Y., 2017. Talanta 174, 521–526.
Liu, M., Wang, Z.Y., Zong, S.F., Chen, H., Zhu, D., Wu, L., Hu, G.H., Cui, Y.P., 2014. ACS Appl. Mater. Interfaces 6, 7371–7379.
Liu, J.L., Tang, Z.L., Zhuo, Y., Chai, Y.Q., Yuan, R., 2017. Anal. Chem. 89, 9108–9115.
Liu, Q., Ma, C., Liu, X.P., Wei, Y.P., Mao, C.J., Zhu, J.J., 2017. Biosens. Bioelectron. 273–279.
Liu, X.Q., Shi, L.H., Niu, W.X., Li, H.J., Xu, G.B., 2007. Angew. Chem. Int. Ed. 46, 421–424.
Lu, J., Getz, G., Miska, E.A., Alvarez-Saavedra, E., Lamb, J., Peck, D., Sweet-Cordero, A., Ebert, B.L., Mak, R.H., Ferrando, A.A., Downing, J.R., Jacks, T., Horvitz, H.R., Golub, T.R., 2005. Nature 435, 834–838.
Lu, L.P., Liu, C., Kang, T.F., Wang, X.Y., Guo, G.S., Miao, W.J., 2018. Sens. Actuators B: Chem. 255, 35–41.
Nie, Y.M., Zhang, P., Wang, H.J., Zhuo, Y., Chai, Y.Q., Yuan, R., 2017. Anal. Chem. 89, 12821–12827.
Oh, J.W., Lee, Y.O., Kim, T.H., Ko, K.C., Lee, J.Y., Kim, H., Kim, J.S., 2009. Angew. Chem. Int. Ed. 48, 2522–2524.
Rashidnadimi, S., Hung, T.H., Wong, K.T., Bard, A.J., 2008. J. Am. Chem. Soc. 130, 634–639.
Shimron, S., Wang, F., Orbach, R., Willner, I., 2012. Anal. Chem. 84, 1042–1048.
Tang, C.X., Zhao, Y., He, X.W., Yin, X.B., 2010. Chem. Commun. 46, 9022–9024.
Venkataraman, S., Dirks, R.M., Rothemund, P.W.K., Winfree, E., Pierce, N.A., 2007. Nat. Nanotechnol. 2, 490–494.
Wang, F., Elbaz, J., Orbach, R., Magen, N., Willner, I., 2011. J. Am. Chem. Soc. 133, 17149–17151.
Wang, F., Elbaz, J., Willner, I., 2012. J. Am. Chem. Soc. 134, 5504–5507.
Wang, H.J., Chai, Y.Q., Li, H., Yuan, R., 2018. Biosens. Bioelectron. 100, 35–40.
Wang, Q., Liu, R.J., Yang, X.H., Wang, K., Zhu, J.Q., He, L.L., Li, Q., 2016. Sens. Actuators B: Chem. 223, 613–620.
Wu, L., Qu, X.G., 2015. Chem. Soc. Rev. 44, 2963–2997.
Wu, X.Y., Chai, Y.Q., Zhang, P., Yuan, R., 2015. ACS Appl. Mater. Interfaces 7, 713–720.
Xu, X.H., Bard, A.J., 1995. J. Am. Chem. Soc. 117, 2627–2631.
Xu, Z.Q., Liao, L.L., Chai, Y.Q., Wang, H.J., Yuan, R., 2017. Anal. Chem. 89, 8282–8287.
Yang, L., Liu, C.H., Ren, W., Li, Z.P., 2012. ACS Appl. Mater. Interfaces 4, 6450–6453.
Yin, B.C., Liu, Y.Q., Ye, B.C., 2012. J. Am. Chem. Soc. 134, 5064–5067.
Yin, X.B., Xin, Y.Y., Zhao, Y., 2009. Anal. Chem. 88, 9299–9305.
Zhang, H., Wang, Y., Zhao, D., Zeng, D., Xia, J., Aldalbahi, A., Wang, C., San, L., Fan, C., Zuo, X., Mi, X., 2015. ACS Appl. Mater. Interfaces 7, 16152–16156.
Zhang, K., Dong, H.F., Dai, W.H., Meng, X.D., Lu, H.T., Wu, T.T., Zhang, X.J., 2016. Anal. Chem. 89, 648–655.
Zhang, P., Zhuo, Y., Chang, Y.Y., Yuan, R., Chai, Y.Q., 2015. Anal. Chem. 87, 10385–10391.
Zhou, W., Tian, Y.F., Yin, B.C., Ye, B.C., 2017. Anal. Chem. 89, 6120–6128.